Int J Thermophys (2009) 30:1918–1930
DOI 10.1007/s10765-009-0688-x

Thermophysical Properties of Electrically Conductive SiC–$(Nb,Ti–C)_{ss}$-Based Cermets

Miroslav Balog · Viliam Vretenár · Ivo Vávra · Jiaming Zhang · Martin A. Crimp · L'udovít Kubičár · Zoltán Lenčéš

Received: 2 December 2008 / Accepted: 19 November 2009 / Published online: 28 November 2009

Abstract Multifunctional cermets are being developed for a range of novel applications. The present paper deals with thermophysical properties of electrically conductive SiC-based cermets. The cermets were prepared by in situ reaction using a two-step sintering process. The thermophysical properties, namely, thermal conductivity, thermal diffusivity, and heat capacity, were measured using the pulse transient technique. The microstructure and chemical composition of the samples were characterized by SEM (scanning electron microscopy), TEM (transmission electron microscopy), STEM (scanning transmission electron microscopy), and EDX (energy dispersive X-ray analysis) techniques. The observed thermophysical data were correlated with the observed microstructures and chemical nature of the SiC-based cermets.

Keywords SiC · Cermets · Thermal conductivity · Thermal diffusivity · Heat capacity · Multifunctional materials · Pulse transient technique

M. Balog
Institute of Materials and Machine Mechanics, Slovak Academy of Sciences, Račianska 75, 831 02 Bratislava, Slovakia

V. Vretenár (✉) · L. Kubičár
Institute of Physics, Slovak Academy of Sciences, Dúbravská 9, 845 11 Bratislava, Slovakia
e-mail: fyzivili@savba.sk

I. Vávra
Institute of Electrical Engineering, Slovak Academy of Sciences, Dúbravská 9, 841 04 Bratislava, Slovakia

J. Zhang · M. A. Crimp
Department of Chemical Engineering and Materials Science, Michigan State University, 2527 Engineering Building, East Lansing, MI 48824-1226, USA

Z. Lenčéš
Institute of Inorganic Chemistry, Slovak Academy of Sciences, Dúbravská 9, 841 04 Bratislava, Slovakia

1 Introduction

The practical utilization of advanced ceramic materials in severe applications is continuously increasing. The main reason for the increased utilization of SiC-based ceramics as structural components in advanced equipment is their superior mechanical and thermophysical properties over a wide range of temperatures [1–9]. Due to this fact, ceramic materials are potential competitors for metal alloys in many technologies. For example, in nuclear reactors SiC-based ceramics may find use in applications typically dominated by metallic-based materials [10,11]. In addition, suitable combinations of ceramics and metals in the form of composites (cermets) can have optimum combinations of properties of both of the precursor materials. Such materials may exhibit extraordinary properties compared to the base components. Currently, most commercially available cermets are Ni- and Co-based [12–14]. The main advantages of these materials are their optimized mechanical properties, especially fracture toughness and electrical properties. Since metals are good at dissipating energy during cracking, metal admixture into ceramic matrices often results in increases in its fracture toughness [15]. However, many of these cermets are limited by their relatively low utilization temperatures due to the low melting temperatures of base metals.

To answer this challenge, a new generation of cermets have been developed [16–18]. Since ceramic materials are typically used for high-temperature applications, high-temperature cermets need to be prepared. SiC-based cermets are strong candidates for these applications due to their extraordinary properties at both room and elevated temperatures.

Currently both SiC and high-temperature structural metals, such as Nb and Ti, are used in the nuclear industry [11,19]. One would expect that cermets based on a combination of these would exhibit enhanced properties. Nevertheless, production of SiC-based cermets may be limited by the relatively high reactivity of SiC with the metals at high temperatures.

The aim of the present work is the detailed characterization of the thermophysical properties of newly produced SiC-based ceramic–metal composites prepared by in situ reaction.

2 Experimental

2.1 Processing and Microstructure Characterization

β-SiC powder (Superior Graphite, USA) was mixed with Y_2O_3 (H.C. Starck, Germany) and AlN (H.C. Starck, Germany) sintering additives, along with Ti (TOHO Titanium Co., Japan) and NbC (Japan New Metals Co., Japan) metallic precursors. The amount of the sintering additives was kept constant at 13 mass% relative to SiC, while the fraction of metallic precursors was varied. The chemical compositions studied are listed in Table 1. The powder mixtures were ball-milled in isopropyl alcohol with SiC balls for 24 h. The homogenized suspensions were dried and subsequently sieved through 25 μm in order to avoid large hard agglomerates. All samples were hot-pressed in two steps: first at 1650 °C for 3 h, and secondly at 1850 °C for 1 h at 30 MPa

Table 1 Chemical composition of samples

Samples	Composition in mass%				
	SiC	AlN	Y_2O_3	Ti	NbC
SC	87	3	10	–	–
SC-10N	78.3	2.7	9	3.60	6.40
SC-20N	69.6	2.4	8	7.14	12.86
SC-50N	43.5	1.5	5	17.85	32.15
SC-80N	17.4	0.6	2	28.55	51.45
N	–	–	–	35.6	64.4

Note: the designation N represents the mass% metal relative to SiC

in an Ar atmosphere. A detailed process description is given elsewhere [20]. Densities were measured by Archimedes' method in mercury. The hot-pressed materials were cut, polished, and plasma etched for microstructure analysis. The microstructures were observed by scanning electron microscopy (SEM). Analytical transmission electron microscopy was performed using a Jeol 2200 FS transmission electron microscopy/scanning transmission electron microscopy (TEM/STEM; acceleration voltage 200 kV, equipped with FEGun and Oxford Instruments EDX system) with an in-column omega filter. Chemical analyses were carried out using energy dispersive X-ray analysis (EDX).

2.2 Thermophysical Characterization

Thermophysical properties were measured by the pulse transient method [21], which belongs to a group of methods known as contact transient methods [22]. The main advantages of the pulse transient method in comparison with classical approaches are both the capability of determining three thermophysical properties, namely, specific heat, thermal diffusivity, and thermal conductivity, within a single experiment, and the use of relatively short measuring times [22,23].

Thermophysical properties can vary in materials prepared under differing thermodynamic processing conditions. Any adjustments that change an atom's surrounding potentials can be identified through thermophysical measurements. While the thermal diffusivity as a transport parameter is sensitive to structural changes and the nature of interfaces between the grains and phases, the specific heat corresponds more to the chemical composition and thermodynamics of the materials. The thermal conductivity, as a product of the thermal diffusivity and specific heat (as shown in Eq. 2 below), includes both aspects.

The principle of the pulse transient method is shown in Fig. 1. The specimen consists of three sections (I, II, III), with a planar heat source clamped between the first and second sections. A heat pulse is produced by Joule heating of an electrical resistor at the planar source. A thermocouple junction is placed between the second and third sections, where the temperature of the second junction is stabilized. The entire experimental setup is thermodynamically isolated to avoid outside influences. A small

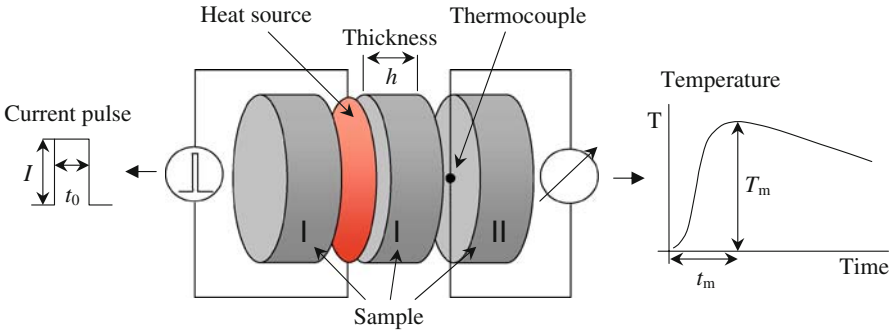

Fig. 1 Experimental setup for the pulse transient method

disturbance in the form of a heat pulse is applied to the specimen, and the thermophysical properties are determined based upon the temperature response as follows.

The material response is characterized by the temperature function [24],

$$T(h,t) = \frac{2q}{c_p \rho \sqrt{a}} \left\{ \sqrt{t} F\left(\frac{h}{2\sqrt{at}}\right) - \sqrt{t-t_0} F\left(\frac{h}{2\sqrt{a(t-t_0)}}\right) \right\}$$
$$F(x) = \frac{1}{\sqrt{\pi}} \exp(-x^2) - x\Phi^*(x), \tag{1}$$

where $q = RI^2$ represents the heat flux supplied by the heat source per unit area, R is the electrical resistance of the heat source, I is the current supplied at time t_0, t is the time, h is the distance between the heat source and the temperature sensor, ρ is the specimen density, and a and c_p are the thermal diffusivity and specific heat, respectively. The symbol Φ^* denotes a complementary error function.

The thermal diffusivity a and specific heat c_p are calculated by superimposing the temperature function, Eq. 1, on the temperature response using an appropriate fitting technique, i.e., Levenberg-Marquant method. The third thermophysical property, thermal conductivity λ, is calculated by the well-known relation,

$$\lambda = a c_p \rho \tag{2}$$

The instrument *RT 1.02* developed by the Institute of Physics SAS, was used for measuring the thermophysical properties. A thermostat in combination with plate heat exchangers established the specimen temperature prior to the heat pulse. This initial temperature was stabilized at (25±0.02) °C. A programmable current source was used for generation of a heat pulse using a planar electrical resistance of 0.5 Ω. The planar heat source was made of copper foil of 20 μm thickness etched in the form of a meander and covered from both sides in thin polyethylene foil 1 μm thick. The temperature response was scanned with a Keithley multimeter. Thermocouple wires (chromel-alumel, Type K) with a thickness of 12 μm were used for a thermometer fabrication. The diameter of the original thermocouple was less than 25 μm. A pc synchronized all units. The typical parameters of the temperature response were $T_m \sim 1$ K and $t_m \sim 1.5$ s.

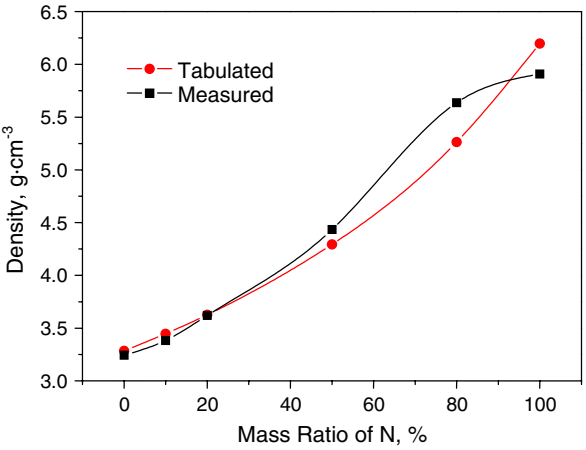

Fig. 2 Measured and theoretical densities of the prepared samples

The samples were prepared in the form of three cylinders (plates) with a diameter of 15 mm, where the thickness of the measured active middle part of each specimen plate was from 2.5 mm to 3 mm. Thermal conductive oil was used to provide good thermal contact between the individual parts of the specimen. Measurement uncertainties, estimated according to the uncertainty budget of the method [25], were up to 8 % for the thermal diffusivity, up to 5 % for the specific heat, and up to 6 % for the thermal conductivity.

3 Results and Discussion

3.1 Density

The measured densities of the prepared cermets are shown in Fig. 2 in comparison with theoretical densities calculated from the densities of the base components. The differences between the theoretical and measured values were found to be up to 7 % for samples with 80 mass% and 100 mass% of metallic phases. Since the densities of all samples, except the pure metallic sample (sample N), are equal to or higher than the theoretical values, it is assumed that the prepared materials are fully dense. This assumption was reinforced by SEM study, which found no significant porosity in any of the samples (Fig. 3), except in the case of the pure metallic sample (sample N), where some small residual porosity was observed. The close correlation between the measured and theoretical densities can be attributed to the development of fine, close-packed phases produced during the sintering process.

3.2 Microstructure and Chemical Analysis

The characteristic microstructures observed by SEM are shown in Fig. 3. The microstructure of sample SC (no metallic precursors, only sintering additives) consists of a large fraction of elongated grains owing to the long sintering time (1650 °C/3h + 1850 °C/1h) in the α-SiC temperature region. In the case of samples with addition of

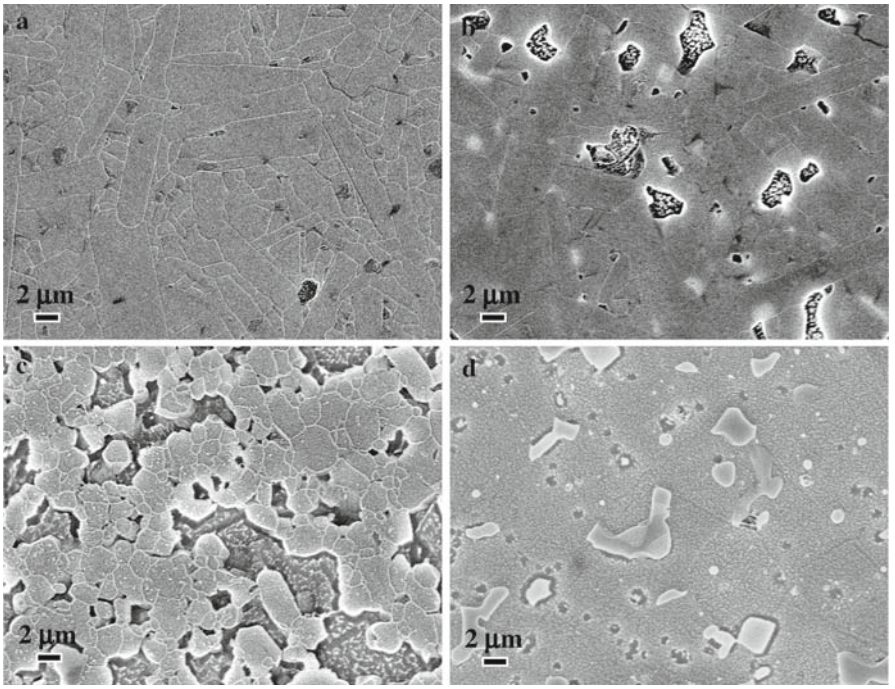

Fig. 3 Scanning electron microscopy secondary electron images showing the microstructures of samples SC-Y, SC-10N, SC-50N, and SC-80N

metallic precursors, additional phases were formed as metallic islands (darker areas). Generally, the presence of new phases has inhibited growth of SiC grains (Fig. 3b–d).

Detailed chemical analyses of the prepared materials illustrate the strong influence of the starting composition on the final chemical composition. The microstructure of sample SC is typical of a high-temperature ceramic consolidated with the aid of sintering agents, consisting of SiC grains and inter-grain phases localized at grain boundaries and triple lines. Detailed STEM/EDX analyses show that grain boundary phases consist of Si, Al, Y, and O (Fig. 4).

The pure metallic sample N was found to consist of only two phases, a (Ti,Nb) solid solution and a (Ti,Nb)C solid solution. These $(Ti,Nb)_{ss}$ and $(Ti,Nb)C_{ss}$ phases are the products of the *in situ* reaction between Ti and NbC (Fig. 5). The formation of these two phases is expected based on the Ti–Nb–C ternary phase diagram [26].

With the addition of the Ti and NbC precursors into SiC/sintering agent components, significantly different microstructural features developed in comparison with the base SiC (sample SC) and pure metallic material (sample N). EDX spectra from sample SC-50N are shown in Fig. 6. The SiC grains were modified by small levels of Ti (Fig. 6c). Additionally, the expected $(Ti,Nb)_{ss}$-based grains were modified by diffusion of Si into the grains (Fig. 6b). The oxygen-based grain boundary phase was modified as well. This grain boundary phase contains Si, O, Y, Al, and Ti, Nb but no C, indicating that the liquid grain boundary phase dissolved Ti during processing (Fig. 6d).

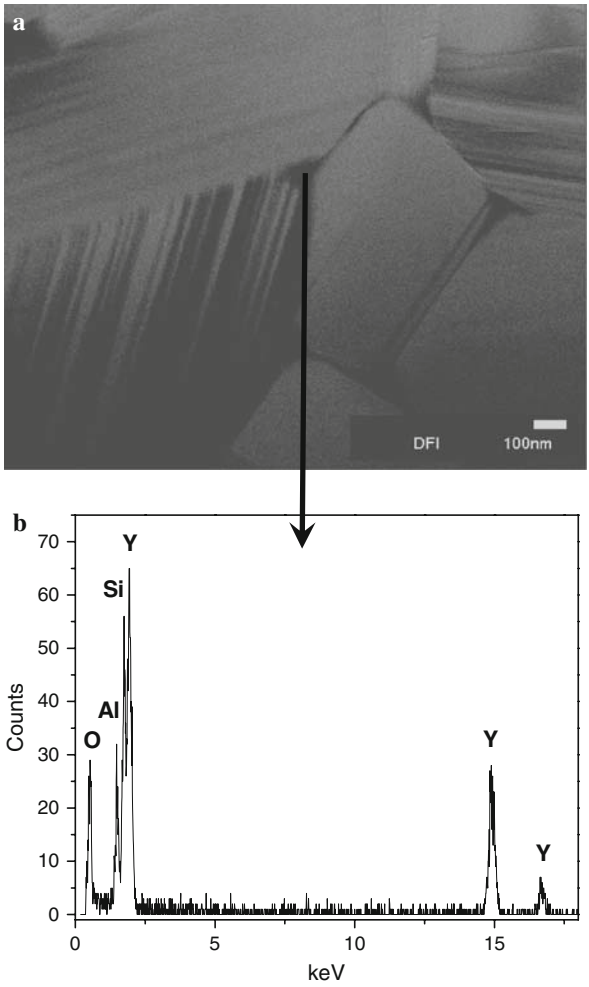

Fig. 4 (**a**) STEM bright field image of sample SC showing large SiC grains (with stacking faults and twins) coated with a distinct grain boundary phase and (**b**) EDX spectrum of the grain boundary phase triple pocket noted

Similar microstructure/chemical nature relationships were identified in the sample SC-80N (Fig. 7). Interestingly, while the amount of metallic and grain boundary phases was a strong function of the metallic precursor level, the chemical nature of these phases was not found to vary with the metallic addition level.

3.3 Thermophysical Properties

The dependence of the measured and calculated specific heats on the mass percent of metallic precursor addition (N) in SiC cermets is depicted in Fig. 8. The calculations were performed using the rule of mixtures based upon the published values for individual components, reported in Table 2. The values of the specific heat linearly decrease with increasing content of the metallic phases from $671\,\mathrm{J\cdot kg^{-1}\cdot K^{-1}}$ to $402\,\mathrm{J\cdot kg^{-1}\cdot K^{-1}}$, in accord with the rule of mixtures. Satisfactory agreement has been

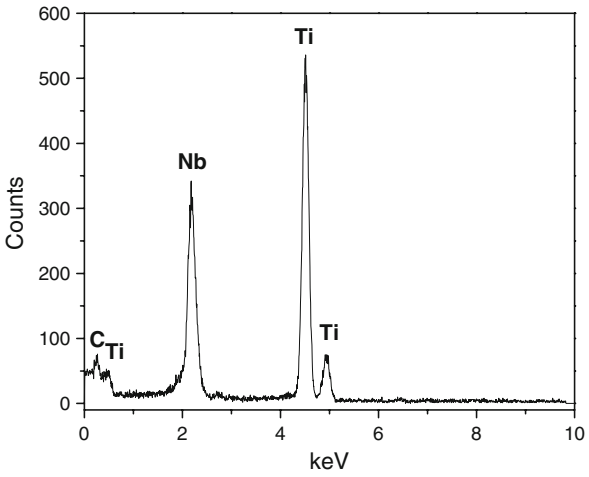

Fig. 5 EDX spectrum of sample N

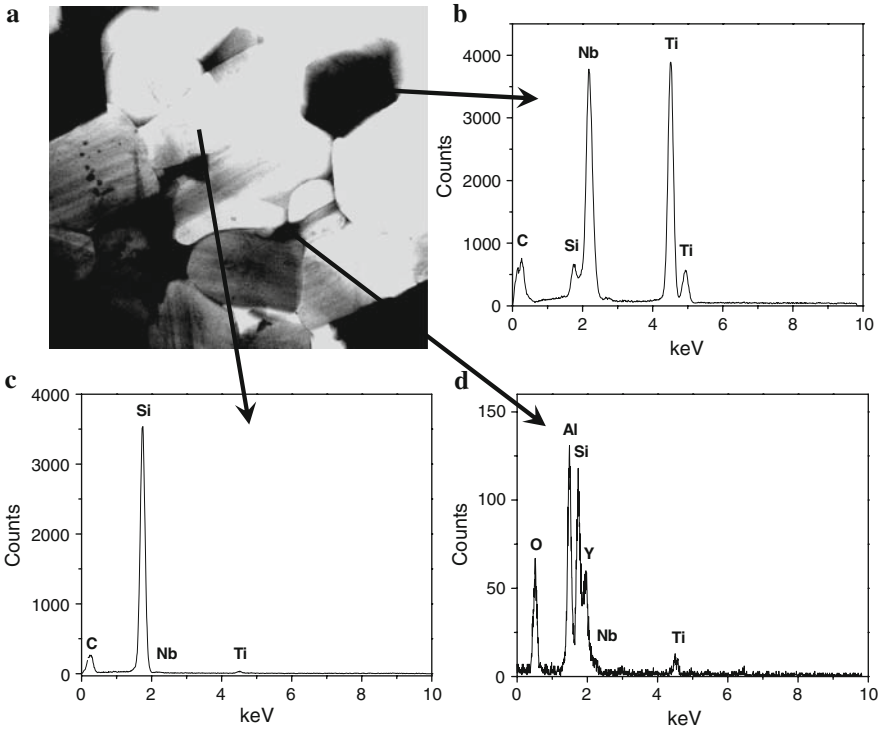

Fig. 6 (**a**) STEM bright field image of sample SC-50N showing SiC grains and metallic grains, (**b**) EDX spectrum of the metallic phases, (**c**) EDX spectrum of the SiC grains, and (**d**) EDX spectrum of the grain boundary phase triple pocket noted

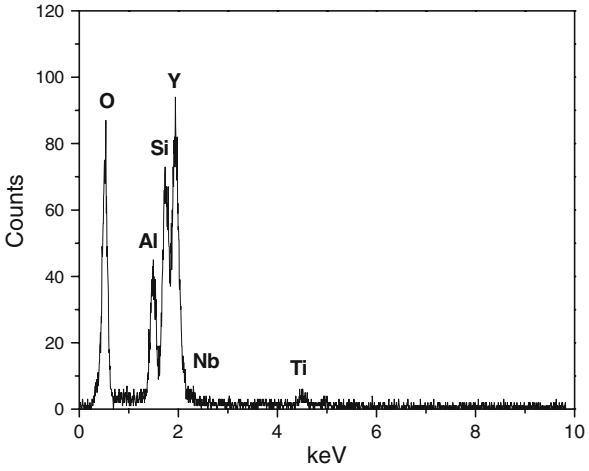

Fig. 7 EDX spectrum of the grain boundary phase in sample SC-80N

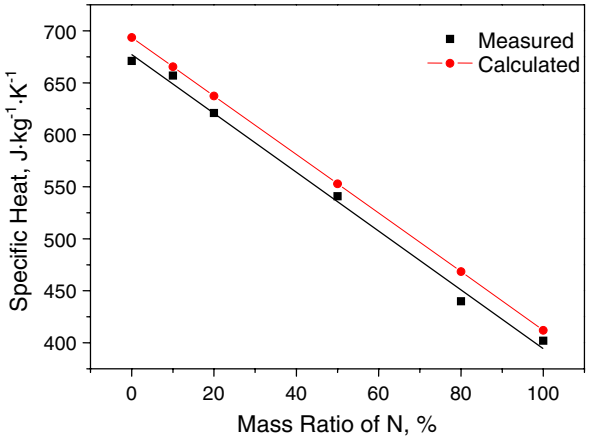

Fig. 8 Measured and calculated specific heats of the SiC-based cermets at 25 °C

found between the measured values and calculated data, with a difference less than 5 %. This implies that the bulk ceramic and metallic phases are the majority phases, and that the specific heat is not sensitive to moderate chemical variations of phases. While the specific heat expresses the accumulated energy per unit mass per degree, a technically more informative property is the volumetric heat capacity (product of the specific heat and density), which expresses an accumulated thermal energy per unit volume per degree. The volumetric heat capacity dependence on the volume ratio of the metallic phase (determined by image analysis of SEM images) in SiC cermets is depicted in Fig. 9. The theoretical values were estimated using the calculated values of specific heats and densities (Figs. 2, 8), with the values of the specific heat were normalized by a value of 17 $J \cdot kg^{-1} \cdot K^{-1}$ (the average shift between measured and calculated values). Contrary to the specific heat, the volumetric heat capacity increases with increasing volume fraction of metallic phases. The maximum volumetric heat

Table 2 Tabulated values of specific heat of individual components at room temperature

Component	SiC	AlN	Y_2O_3	Ti	NbC
Specific heat ($J \cdot kg^{-1} \cdot K^{-1}$)	714 [28]	900 [28]	454 [29]	523 [27]	351 [28]

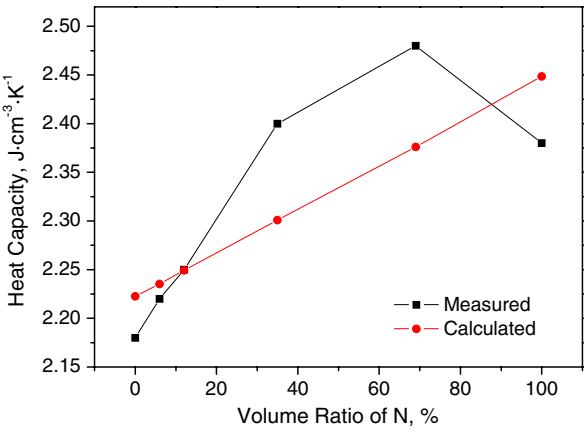

Fig. 9 Measured and theoretical volumetric heat capacities of the SiC-based cermets at 25 °C

capacity of $2.47\,J \cdot cm^{-3} \cdot K^{-1}$ was found for the sample with 80 mass% of metallic phases. The non-linear behavior correlates with the observed density discrepancies (Fig. 2) created by modified chemical composition of majority phases compared with the pure samples SC and N, respectively. Hence, SiC doped with Ti and $(Nb,Ti)C_{ss}$ doped with Si are responsible for the volumetric heat-capacity enhancement. Additionally, the volumetric heat capacity may be partially affected by the modified grain boundary phase due to the reaction with the metallic precursors (Fig. 6 d). During the processing, the metallic components (particularly Ti) dissolved and diffused into the liquid grain boundary phase, resulting in the grain boundaries being enriched in Ti. The presence of metals may result in enhancement of the volumetric heat capacity of the grain boundary phase. Consequently, the overall heat capacity increases.

The thermal diffusivity is particularly affected by the metallic phases developed in the SiC-based samples, as seen in Fig. 10. While samples SC, SC-10N, and SC-20N nearly have the same thermal diffusivity of about $22 \times 10^{-6}\,m^2 \cdot s^{-1}$, increasing fractions of metallic phases result in an order-of-magnitude decrease in the thermal diffusivity to $2.63 \times 10^{-6}\,m^2 \cdot s^{-1}$. The maximum change in thermal diffusivity occurred between 50 mass% and 80 mass% metallic precursor addition, which can be correlated to the density and chemical composition. Here again, the structural and chemical changes of the materials are the most important factors in determining the thermophysical behavior.

Since the thermal conductivity is a product of the specific heat and thermal diffusivity, Eq. 2, it is clear that it will follow the curve of thermal diffusivity (Fig. 11, compare with Fig. 10). The thermal conductivity remains approximately constant at about $49\,W \cdot m^{-1} \cdot K^{-1}$ with up to 20 mass% of metal precursor addition in SiC. Above this level, it decreases to $6.25\,W \cdot m^{-1} \cdot K^{-1}$ for pure metallic precursor sample N.

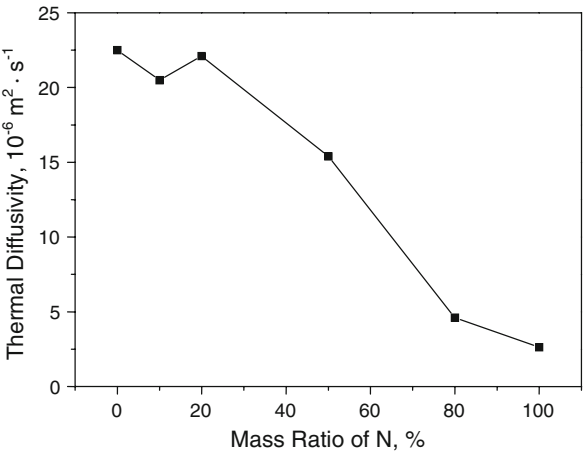

Fig. 10 Experimentally determined thermal diffusivity of the SiC-based cermets at 25 °C

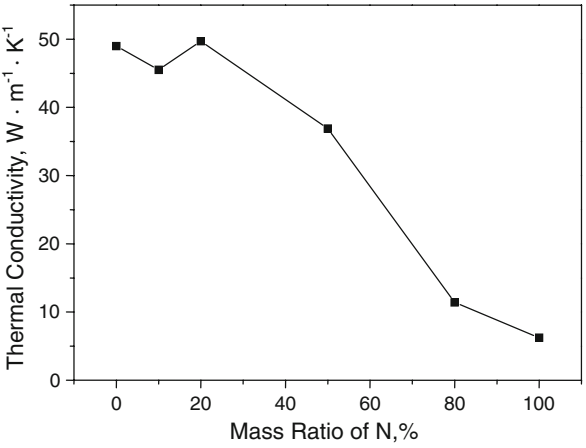

Fig. 11 Experimentally determined thermal conductivity of the SiC-based cermets at 25 °C

Table 3 Tabulated values of thermal conductivity of individual components at room temperature

Component	SiC	AlN	Y_2O_3	Ti	NbC
Thermal conductivity ($W \cdot m^{-1} \cdot K^{-1}$)	43–145 [28]	180–220 [28]	27 [30]	21.9 [27]	14.2 [28]

Based upon the minimum thermal conductivity approximation and considering only the main components of the samples, the reference values (Table 3) for SC and N samples were estimated to be around 43 $W \cdot m^{-1} \cdot K^{-1}$ and 14.2 $W \cdot m^{-1} \cdot K^{-1}$, respectively. The low value of our N sample is probably due to phonon scattering on the grain and interphase boundaries of the metallic phases. Also, the modified chemistries of Ti and NbC may play a role in affecting the thermal scattering.

The observed plateau in the measured thermal conductivity and thermal diffusivity at small mass ratios of N was due to the predominant effect of the SiC

phase and/or chemical changes that occurred during the processing. At these relatively low metal levels, the metallic phases have limited influence on the thermal conductivity. Above a critical level of metallic additions (higher than 20 mass%), the thermophysical properties are modified by metallic-based phases. Therefore, a decrease in thermal conductivity and thermal diffusivity was observed.

The experimental measurements of the thermophysical properties of SiC-based cermets show strong dependence on metal content. As expected, the volumetric heat capacity is more sensitive to chemical composition than the specific heat.

Interestingly, the improvement of other properties of these SiC cermets (for example, the electrical conductivity [20]) is at the expense of their heat transport properties. Thus, in many applications it may be necessary to reach a compromise between the ideal thermal and electrical properties. In order to avoid the total degradation of thermophysical properties, the metallic content in SiC cermets should not exceed a limit of ∼50 mass%, where the thermal conductivity has dropped by approximately 20 %. Beyond ∼50 mass% N (see Figs. 10, 11), the thermal conductivity drops-off rapidly.

4 Conclusions

The thermophysical properties of SiC-based cermets modified by the addition of metallic phase precursors have been studied at room temperature.

The specific heat linearly decreases with increasing fraction of metallic phases in accordance with the rule of mixtures, while the thermal diffusivity and thermal conductivity are relatively constant up to 20 mass% of metallic precursors. This plateau in the thermal conductivity and diffusivity was due to the predominant effect of the phonon transport between the SiC grains. Further increase in metallic content resulted in rapidly decreasing thermal diffusivity. The maximum change in the thermal diffusivity was observed between 50 mass% and 80 mass% of metallic content.

The volumetric heat capacity increases with increasing content of the volume fraction of the metallic phase. A maximum volumetric heat capacity of $2.47\,\mathrm{J\cdot cm^{-3}\cdot K^{-1}}$ was exhibited at 80 mass% of metallic addition due to the presence of intermediate phases compared with the pure metallic and ceramic samples. In addition, the SiC grains were modified by diffusion of Ti into the grains. Likewise, the (Nb,Ti)C_{ss}-based grains were altered by dissolution of Si into this phase. Consequently, the volumetric heat capacity may be affected by the chemical modification of the various phases, in particular, the grain boundary phases.

Acknowledgments Financial support of the Slovak Grant Agency, Project Nos. VEGA 2/4072/24, and Centre of Excellence NANOSMART and of the J. Fulbright Commission in the Slovak Republic is gratefully acknowledged. The JEOL 2200 FX used in this study was purchased using funds from the U.S. National Science Foundation.

References

1. S.J. Schneider, *Engineered Materials Handbook*, vol. 4 (ASM International, Materials Park, 1987)
2. L. Fa, Z. Dongmei, S. Xiaolei, Z. Wancheng, Mater. Sci. Eng. A **458**, 7 (2007)
3. S.P. Lee, Y.S. Shin, D.S. Bae, B.H. Min, J.S. Park, A. Kohyama, Fusion Eng. Des. **81**, 963 (2006)
4. Y. Morisada, Y. Miyamoto, Y. Takaura, K. Hirota, N. Tamari, Int. J. Refract. Met. Hard Mater. **25**, 322 (2007)
5. Y. Zhou, K. Hirao, K. Watari, Y. Yamauchi, S. Kanzaki, J. Eur. Ceram. Soc. **24**, 265 (2004)
6. L.S. Sigl, J. Eur. Ceram. Soc. **23**, 1115 (2003)
7. E. Volz, A. Roosen, W. Hartung, A. Winnacker, J. Eur. Ceram. Soc. **21**, 2089 (2001)
8. H. Nakano, K. Watari, Y. Kinemuchi, K. Ishizaki, K. Urabe, J. Eur. Ceram. Soc. **24**, 3685 (2004)
9. L.L. Snead, J. Nucl. Mater. **329**, 524 (2004)
10. A. Möslang, T. Wiss, Nat. Mater. **5**, 679 (2006)
11. Y. Katoh, L.L. Snead, C.H. Henager Jr., A. Hesegawa, A. Kohyama, B. Riccardi, H. Hegeman, J. Nucl. Mater. **367**, 659 (2007)
12. J. Zackrisson, H.O. Andrén, Int. J. Refract. Met. Hard Mater. **17**, 265 (1999)
13. H.C. Kim, I.J. Shon, J.K. Yoon, J.M. Doh, Z.A. Munir, Int. J. Refract. Met. Hard Mater. **24**, 427 (2006)
14. K. Cai, C.W. Nan, X.M. Min, Mater. Res. Bull. **32**, 1327 (1997)
15. O. Raddatz, G.A. Schneider, W. Mackens, H. Voss, N. Claussen, J. Eur. Ceram. Soc. **20**, 2261 (2000)
16. F. Monteverde, V. Medri, A. Bellosi, J. Eur. Ceram. Soc. **22**, 2587 (2002)
17. N. Liu, W. Yin, L. Zhu, Mater. Sci. Eng. **A 445**, 707 (2007)
18. H. Zhang, J. Yan, X. Zhang, S. Tang, Int. J. Refract. Met. Hard Mater. **24**, 236 (2006)
19. K. Ozawa, T. Nozawa, Y. Katoh, T. Hinoki, A. Kohyama, J. Nucl. Mater. **367**, 713 (2007)
20. M. Balog, P. Šajgalík, F. Hofer, P. Warbichler, K. Fröhlich, O. Vávra, J. Janega, J.L. Huang, J. Eur. Ceram. Soc. **26**, 1259 (2006)
21. L'. Kubičár, in *Pulse Method of Measuring Basic Thermophysical Parameters*, ed. by G. Svehla. Comprehensive Analytical Chemistry, Vol. XII, Thermal Analysis, Part E (Elsevier, Amsterdam, Oxford, New York, Tokyo, 1990), p. 1350
22. L'. Kubičár, V. Boháč, Review of several dynamic methods of measuring thermophysical parameters, in *Proceedings of 24th Int. Conf. on Thermal Conductivity/12th Int. Thermal Expansion Symposium*, ed. by P.S. Gaal, D.E. Apostolescu (Technomic Pub. Co., Lancaster, Pennsylvania,1999), pp. 135–149
23. K.D. Maglić, A. Cezairliyan, V.E. Peletsky, *Compendium of Thermophysical Property Measurement Methods, Vol. 2, Recommended Measurement Techniques and Practices* (Plenum Press, New York, 1992), p. 643
24. H.S. Carslaw, J.C. Jaeger, *Conduction of Heat in Solids*, 2nd edn. (Oxford University Press, Oxford, 1959), p. 496
25. L'. Kubičár, V. Vretenár, V. Boháč, P. Tiano, Int. J. Thermophys. **27**, 220 (2006)
26. A.E. McHale, *Phase Equilibria Diagrams*, vol. X (The American Ceramics Society, Westerville, 1994)
27. D.R. Lide, *CRC Handbook of Chemistry and Physics* (CRC Press, Boca Raton, FL, 2005). http://www.hbcpnetbase.com
28. H.O. Pierson, *Handbook of Refractory Carbides and Nitrides* (William Andrew Publishing/Noyes, Norwich, 1996), p. 362
29. J.A. Dean, *Lange's Handbook of Chemistry*, 15th edn. (McGraw-Hill, New York, 1999)
30. P.H. Klein, W.J. Croft, J. Appl. Phys. **38**, 1603 (1967)